The Journal of Chemical Physics

RESEARCH ARTICLE | DECEMBER 12 2023

Recombination statistics of nonionic surfactant micelles at equilibrium

Yusuke Koide

J. Chem. Phys. 159, 224906 (2023)
https://doi.org/10.1063/5.0175946

The Journal of Chemical Physics ARTICLE pubs.aip.org/aip/jcp

Recombination statistics of nonionic surfactant micelles at equilibrium

Cite as: J. Chem. Phys. 159, 224906 (2023); doi: 10.1063/5.0175946
Submitted: 10 September 2023 • Accepted: 21 November 2023 •
Published Online: 12 December 2023

Yusuke Koide[a)]

AFFILIATIONS

Graduate School of Engineering Science, Osaka University, 1-3 Machikaneyama, Toyonaka, Osaka 560-8531, Japan

[a)]Author to whom correspondence should be addressed: y_koide@fm.me.es.osaka-u.ac.jp

ABSTRACT

We conduct dissipative particle dynamics simulations of nonionic surfactant solutions to investigate the statistical properties of micellar recombination. We categorize the recombination events into self-recombination, where two micelles created by scission join together, and non-self-recombination. We find that these two recombination events exhibit distinct statistical properties. The probability density function of the recombination time for self-recombination follows a power law, and we show that the mean squared displacement of the surfactants determines the exponent of the power law. In contrast, the survival function for non-self-recombination is exponential, which is consistent with the mean-field model. For non-self-recombination, we evaluate the mean recombination time for various aggregation numbers, temperatures, and surfactant volume fractions. We find a scaling law describing the mean recombination time of the micelles at equilibrium.

I. INTRODUCTION

Surfactants consist of hydrophilic and hydrophobic moieties and typically self-assemble into micelles in aqueous solutions. In particular, wormlike micelles have been the subject of many rheological studies because they exhibit viscoelasticity similar to that of polymers.[1–3] However, unlike polymers, wormlike micelles exhibit constant scission and recombination.[4] These scission and recombination kinetics result in unique rheological properties. For example, the linear viscoelasticity of concentrated micellar solutions is well described by the Maxwell model.[4–7]

Over the last few decades, several theories have been proposed to explain the rheological properties of wormlike micelle solutions. Cates[4] derived the relaxation time of concentrated micellar solutions from the reptation time and lifetime under the assumption that scission and recombination events are uncorrelated, which corresponds to the mean-field treatment of recombination. However, O'Shaughnessy and Yu[8] theoretically demonstrated that such mean-field treatments sometimes break down. They defined self-recombination as the process in which two chain ends created by scission recombine with their original partner. They found that the distribution function of the recombination time exhibits a power law when self-recombination is the dominant mechanism. In addition, they showed that self-recombination leads to an algebraic decay of stress relaxation at short time scales. Nyrkova and Semenov[9] also theoretically demonstrated that strong correlations between chain scission and recombination result in nonexponential stress relaxation. Therefore, it is imperative to consider self-recombination in order to understand the rheological properties of micellar solutions[10] and develop mesoscopic models.[11]

O'Shaughnessy and Yu's theory[8] was verified using coarse-grained molecular simulations of polymer-like linear chains with scission and recombination kinetics. Padding and Boek[12] conducted molecular simulations of concentrated micellar solutions using the FENE-C model,[13] where scission and recombination are introduced into the finitely extensible nonlinear elastic (FENE) potential. They numerically demonstrated that parameter regimes exist in which self-recombination predominates at short time scales, as predicted by O'Shaughnessy and Yu.[8] The authors of the work of Huang *et al.*[14] modeled micelles using linear chains with a stochastic kinetic model for scission and recombination. They reported that in semidilute solutions, the probability density function of the recombination time for self-recombination follows a power law whose exponent is consistent with the theory.[8] The authors of the work of Thakur *et al.*[15] proposed a coarse-grained model in which the internal structure of micelles is ignored and the wormlike micelle is represented

by a string of trimers. They showed that the probability density function of the recombination time exhibits a crossover from an exponential function to a power law when the system undergoes a transition from the fluid to the gel phase. However, in these previous studies, the recombination process was explicitly modeled based on several phenomenological assumptions. For instance, in some models, recombination occurs only at chain ends; thus, these models are limited to linear chains. In addition, the above-mentioned models ignore complicated internal structures of micelles. Therefore, the statistical properties of more realistic micelles formed through the self-assembly of surfactant molecules remain unclear.

Self-assembly of surfactants has been extensively studied using molecular simulations.[16–24] Sangwai and Sureshkumar[21] employed the coarse-grained molecular dynamics (CGMD) method to reveal the recombination process of two spherical micelles. The authors of the work of Liu *et al.*[24] reported typical recombination processes of surfactant micelles using CGMD. Although recent molecular simulations have investigated the recombination dynamics of micelles, only few studies have been conducted on the statistical properties of recombination.[25] One major issue is the high computational cost of obtaining large amounts of micellar recombination data.

We overcome this difficulty by using the dissipative particle dynamics (DPD) method.[26–28] Owing to coarse-graining and soft repulsive interactions, DPD allows simulations of large systems over long time scales at a low computational cost. Furthermore, surfactant and water molecules are explicitly considered. Thus, we can investigate the statistical properties of the recombination of micelles composed of surfactants. In other words, we do not use an explicit kinetic model for micelles. However, the definition of the recombination time is not clear for micelles composed of surfactants. For the bead–spring chains used in previous studies,[12,14] recombination is defined as the formation of a bond between the two arms of the beads. In contrast, because we do not rely on a bead–spring model, the conventional recombination definition cannot be applied to our system. In this study, we first consider the definition of recombination applicable to the micelles considered. Then, we classify the recombination events into two categories: self-recombination, where two micelles created by scission join together, and non-self-recombination. We demonstrate that the two types of recombination events in surfactant micelles exhibit qualitatively different statistical properties, as predicted by O'Shaughnessy and Yu.[8] Furthermore, we discover a scaling law for the mean recombination time by conducting DPD simulations at various temperatures and surfactant volume fractions.

II. METHOD

A. DPD governing equations

In this study, we use the DPD method to conduct mesoscopic simulations of nonionic surfactant solutions. In DPD simulations, a single DPD particle represents a group of atoms and molecules. The motion of the DPD particle obeys Newton's equation of motion. There are four types of forces: conservative, dissipative, random, and bonded. Further details of the DPD method have been described in previous studies.[29,30] In the following, all quantities are nondimensionalized by $k_B T_0$, m, and r_c, where k_B is the Boltzmann constant, T_0 is the reference temperature, m is the mass of the DPD particle, and r_c is the cutoff distance.

B. Surfactant model

The model of a nonionic surfactant molecule contains a hydrophilic head particle and two hydrophobic tail particles, which are connected by harmonic springs expressed as

$$\boldsymbol{F}_{ij}^{B} = -k_s(|\boldsymbol{r}_{ij}| - r_{\mathrm{eq}})\boldsymbol{e}_{ij}, \tag{1}$$

where k_s is the spring constant, r_{eq} is the equilibrium bond distance, $\boldsymbol{r}_{ij} = \boldsymbol{r}_i - \boldsymbol{r}_j$, and $\boldsymbol{e}_{ij} = \boldsymbol{r}_{ij}/|\boldsymbol{r}_{ij}|$ with $\boldsymbol{r}_i$ being the position of the ith particle. Table I lists the simulation parameters for surfactant solutions. Here, N is the total number of DPD particles, ρ is the number density of DPD particles, σ is the random force coefficient, and a_{ij} is the conservative force coefficient between the different types of particles. The subscripts indicate the particle types, and h, t, and w denote the head, tail, and water particles, respectively.

C. Simulation details

To integrate the equations of motion, we use the modified velocity Verlet method[28] with the time step $\Delta t = 0.04$ and the parameter $\lambda = 0.65$ introduced in this algorithm. We have confirmed that these parameters achieve sufficiently accurate temperature control. We impose a random initial configuration and conduct simulations for 20 000–40 000 time units depending on the parameters, achieving statistically steady values of the potential energy and the number of micelles. All the analysis is done after this initial equilibration. We implement a systematic parameter survey by changing the temperature T and surfactant volume fraction ϕ. When we vary T, the dissipative force coefficient γ changes to satisfy $\sigma^2 = 2\gamma k_B T$ while fixing the value of σ at 3. We perform all the DPD simulations using our in-house code.

D. Analysis details

We need to identify the micelles in the system to evaluate individual micellar properties. We define micelles adopting a method used in previous studies.[31,32] In this method, two surfactant molecules belong to a common cluster if a hydrophobic particle of one surfactant molecule is within $r_c(=1)$ of a hydrophobic particle of the other. If a cluster has an aggregation number N_{ag} that is larger than a threshold value $n_{\mathrm{mic}}(=10)$, the cluster is regarded as a micelle.

To focus on the micellar properties for a fixed N_{ag}, we use conditional statistics based on N_{ag} instead of statistics for all the micelles in the system. Specifically, when evaluating the properties of micelles with N_{ag}, we use the data for micelles with aggregation numbers that lie within $[N_{\mathrm{ag}} - \Delta N_{\mathrm{ag}}, N_{\mathrm{ag}} + \Delta N_{\mathrm{ag}}]$, where we set $\Delta N_{\mathrm{ag}} = 0.05 N_{\mathrm{ag}}$.

TABLE I. DPD simulation parameters for surfactant solutions. N is the total number of DPD particles, ρ is the number density of DPD particles, σ is the random force coefficient, k_s is the spring constant, r_{eq} is the equilibrium bond distance, and a_{ij} is the conservative force coefficient between the different types of particles. The subscripts indicate the particle types, and h, t, and w denote the head, tail, and water particles, respectively.

N	ρ	σ	k_s	r_{eq}	a_{hh}	a_{ht}	a_{hw}	a_{tt}	a_{tw}	a_{ww}
648 000	3	3	50	0.8	25	60	20	25	60	25

III. RESULTS

In this section, we demonstrate that micellar recombination events consist of two types (self-recombination and non-self-recombination) with distinct statistical properties. We then evaluate the characteristic timescale of non-self-recombination and show its dependence on the aggregation number, temperature, and surfactant volume fraction. Before delving into the details of recombination, we briefly describe the characteristics of our system. As reported in our previous paper,[29] the structures of surfactant micelles depend on the aggregation number N_{ag}. Specifically, micelles are spherical for $N_{ag} \lesssim 50$, rodlike for $50 \lesssim N_{ag} \lesssim 200$, and wormlike for $N_{ag} \gtrsim 200$. Note that micelles can form branched structures, especially for large N_{ag}, which is a crucial difference from previous studies.[12,14] Incidentally, there is no entanglement effect in the considered system.[29,30]

A. Two types of recombination events

Herein, we demonstrate two types of recombination events that exhibit qualitatively different statistical properties. First, we define the recombination events in the micelles. We judge that recombination occurs when the aggregation number N_{ag} of a micelle increases by more than the threshold value $n_{mic}(=10)$ at a certain time interval $\delta t(=100\Delta t)$. Similarly, we judge that scission occurs when N_{ag} of a micelle decreases by more than n_{mic} during δt. In previous studies using bead–spring models with scission and recombination kinetics,[12,14] the recombination time t_r was defined for chain ends. However, because the chain ends are not uniquely determined in the case of the micelles considered, we cannot easily adopt the same definition of t_r. Therefore, we define t_r for each micelle. In the present study, t_r is defined as the time between micellar birth and recombination. In the following, t_r is conditioned by the value of N_{ag} before recombination in the conditional analysis defined in Sec. II D. In other words, t_r is the time required for a micelle with N_{ag} to recombine with another micelle. According to the previous study,[8] recombination events can be classified into two types. The first is self-recombination, in which two micelles created by scission are combined. Note that our definition of self-recombination in micelles is not necessarily identical to the original definition of self-recombination in chain ends.[8,12,14] For instance, our definition does not include a case in which one of the two micelles created by scission undergoes scission before recombining with its original partner. The other type of recombination is non-self-recombination. This type of recombination includes an event where one of the two micelles created by scission recombines with a micelle other than the original partner and one where a micelle created by recombination undergoes recombination in succession. Figure 1 shows a self-recombination process, and Fig. 2 illustrates a non-self-recombination process. In particular, Fig. 2 corresponds to an event in which one of the two micelles created by scission recombines with a micelle other than its original partner. In the following, we demonstrate that the two types of recombination follow different statistical laws; thus, they should be distinguished when analyzing recombination time.

We investigate the statistical properties of self-recombination and non-self-recombination. Specifically, we evaluate the survival function $S(t)$, which gives the probability that recombination occurs beyond a certain time t, for each type of recombination

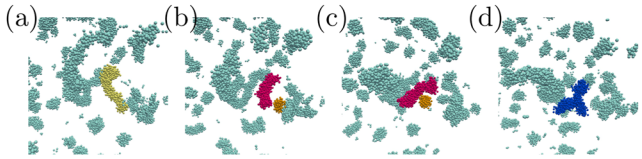

FIG. 1. An example of the self-recombination process. The snapshots correspond to configurations at (a) $t = t_0$, (b) $t_0 + 88$, (c) $t_0 + 216$, and (d) $t_0 + 300$, where t_0 is the start time of visualization. The micelle in yellow breaks into the micelles in pink and orange. Then they recombine and form the micelle in blue.

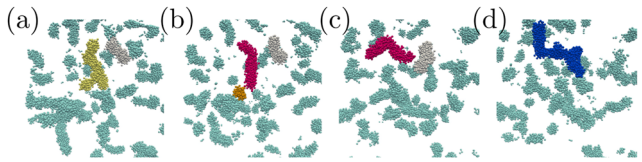

FIG. 2. An example of the non-self-recombination process. The snapshots correspond to configurations at (a) $t = t_0$, (b) $t_0 + 88$, (c) $t_0 + 1000$, and (d) $t_0 + 1184$, where t_0 is the start time of visualization. The micelle in yellow breaks into the micelles in pink and orange. Then, the micelle in pink and the micelle other than the original partner in white recombine and form the micelle in blue.

event using the Kaplan–Meier method.[33] $S_{self}(t)$ and $S_{non\text{-}self}(t)$ denote the survival function for self-recombination and non-self-recombination, respectively. Here, $t_r^{(1)} < t_r^{(2)} < \cdots < t_r^{(n)}$ denote the obtained recombination times of the considered type of recombination. We define d_j as the number of considered events observed at $t_r^{(j)}$ and r_j as the number of individuals surviving just before $t_r^{(j)}$. Then, we obtain

$$S(t) = \prod_{\{j:t_r^{(j)} \le t\}} \left(1 - \frac{d_j}{r_j}\right) \tag{2}$$

using the Kaplan–Meier method. Note that in the Kaplan–Meier method, r_j includes not only individuals that experience the considered event but also those that experience the other events. For example, when estimating $S_{self}(t)$, r_j also includes individuals that finally experience non-self-recombination or scission at $t \ge t_r^{(j)}$. Figure 3(a) shows $S_{self}(t)$ and $S_{non\text{-}self}(t)$ of micelles with $N_{ag} = 300$ with the 95% confidence intervals obtained using the exponential Greenwood formula.[34] Here, we also show the survival function $S_{rec}(t)$ without conditioning the type of recombination for comparison. It should be emphasized that we focus on a statistically steady state, where scission and recombination constantly occur. To estimate the survival function with sufficient accuracy, we perform DPD simulations for 20 000–280 000 time units after initial equilibration, depending on the parameters. For instance, the numbers of self-recombination and non-self-recombination events to obtain $S_{self}(t)$ and $S_{non\text{-}self}(t)$ shown in Fig. 3(a) are 2010 and 4405. Figure 3(a) shows that the survival function is qualitatively different for different types of recombination. Except for short times, $S_{non\text{-}self}(t)$ obeys an exponential function, indicating mean-field behavior.[8] This exponential decay of $S_{non\text{-}self}(t)$ is consistent with the results of bead–spring models with scission and recombination kinetics.[12,14] We evaluate the mean recombination time τ_r by fitting $S_{non\text{-}self}(t)$ to $C_0 \exp(-t/\tau_r)$

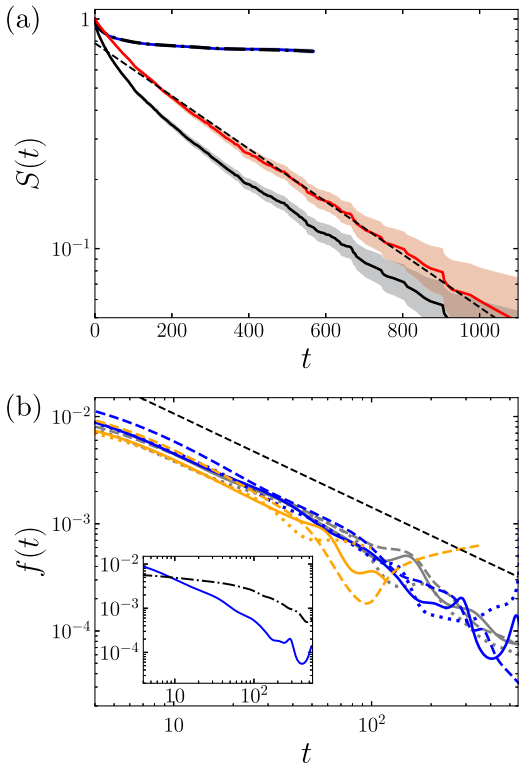

FIG. 3. (a) Survival function $S(t)$ of micelles with $N_{ag} = 300$ for $k_BT = 1$ and $\phi = 0.05$ with the 95% confidence interval: black line, all the recombination events $S_{rec}(t)$; blue line, self-recombination events $S_{self}(t)$; red line, non-self-recombination events $S_{non\text{-}self}(t)$. The black dashed line in (a) is an exponential fit to $S_{non\text{-}self}(t)$. The black dash-dotted line in (a) indicates the Bezier curve approximating $S_{self}(t)$. (b) Probability density function $f_{self}(t)$ of the recombination time for self-recombination with $N_{ag} = 200$ (dashed), 300 (solid), and 400 (dotted) for $(k_BT, \phi) = (0.9, 0.03)$ (gray), (1,0.05) (blue), and (1.2,0.08) (orange). The black dashed line in (b) indicates $f_{self}(t) \propto t^{-7/8}$. The inset in (b) shows $f_{self}(t)$ (blue line) and $f_{non\text{-}self}(t)$ (black dash-dotted line) for $N_{ag} = 300$, $k_BT = 1$, and $\phi = 0.05$.

as shown in Fig. 3(a) because non-self-recombination contributes to the effective recombination of micelles. We will demonstrate the dependence of τ_r on the various parameters in Sec. III B.

Next, we examine the statistical properties of self-recombination. Figure 3(a) shows that $S_{self}(t)$ does not exhibit exponential decay. To discuss the detailed properties of self-recombination, we also evaluate the probability density function $f(t)$ of the recombination time using the relation $f(t) = -S'(t)$. To evaluate the first derivative $S'(t)$ of $S(t)$, we rely on the Bezier curve, which approximates $S(t)$[35] as shown in Fig. 3(a), because $S(t)$ obtained using the Kaplan–Meier method is a step function. Figure 3(b) shows the probability density function $f_{self}(t)$ of the recombination time for self-recombination for several N_{ag}, k_BT, and ϕ. We find that regardless of these parameters, $f_{self}(t)$ obeys a power law $f_{self}(t) \propto t^{-7/8}$ in the intermediate timescales instead of the exponential distribution observed for non-self-recombination [see the inset of Fig. 3(b)]. O'Shaughnessy and Yu[8] predicted that when self-recombination predominates, $f(t)$ is proportional to the second time derivative of $\langle \Delta r^2(t) \rangle^{3/2}$, where $\langle \Delta r^2(t) \rangle$ is the mean squared displacement (MSD) of the chain end. Previous studies[12,14] numerically confirmed this relationship for polymer-like linear chains with scission and recombination kinetics in the concentrated and semidilute regimes. Figure 4 shows the compensated MSD $\langle \Delta r^2(t) \rangle / t^{3/4}$ of the center of mass of the surfactant molecules for various ϕ and k_BT. With regard to polymer chains, the Zimm model[36] predicts that subdiffusive motion emerges in intermediate timescales $\tau_0 < t < \tau$, where τ_0 is the monomer relaxation time, and τ is the longest relaxation time of the chains.[37] We find that the surfactant molecules for the considered parameters show $\langle \Delta r^2(t) \rangle \propto t^{3/4}$ in the intermediate timescales. In fact, the observed subdiffusive regimes are consistent with the longest relaxation time of micelles reported in our previous study.[29] As the relation $\frac{d^2}{dt^2} \langle \Delta r^2(t) \rangle^{3/2} \propto t^{-7/8}$ holds, the observed power law $f_{self}(t) \propto t^{-7/8}$ in intermediate timescales is consistent with the prediction of O'Shaughnessy and Yu.[8] They also theoretically demonstrated that the dominance of self-recombination alters the relaxation behavior of wormlike micelle solutions. To investigate the competition between self-recombination and non-self-recombination, we show $f_{self}(t)$ and $f_{non\text{-}self}(t)$ for fixed N_{ag}, k_BT, and ϕ in the inset of Fig. 3(b). In this case, non-self-recombination predominates over self-recombination for $10 \lesssim t \lesssim 500$. Note that the competition depends on the values of N_{ag}, k_BT, and ϕ. Thus, it is an important near-future study to investigate the effect of self-recombination on the micellar dynamics and rheological properties, although the present study focuses on the recombination statistics of micelles. In summary, we explicitly distinguished between self-recombination and non-self-recombination in surfactant micelles and demonstrated that the two recombination events are described by distinct statistical laws.

Before closing this subsection, we discuss the effect of time interval δt. Because self-recombination frequently occurs at short times, as expected from $f_{self}(t) \propto t^{-7/8}$, δt may significantly influence the results. To verify the robustness of the statistical properties of self-recombination and non-self-recombination, we present $S_{non\text{-}self}(t)$ and $f_{self}(t)$ for various δt values in Fig. 5. Figure 5(a) shows that $S_{non\text{-}self}(t)$ slightly depends on δt. When non-self-recombination occurs after undergoing a set of scission and self-recombination within δt, the recombination time of the micelle is overestimated. Therefore, it is reasonable that $S_{non\text{-}self}(t)$ increases with δt. However, the qualitative behavior of $S_{non\text{-}self}(t)$ and τ_r

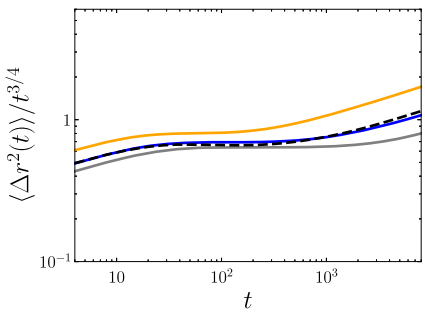

FIG. 4. Compensated MSD $\langle \Delta r^2(t) \rangle / t^{3/4}$ of the center of mass of surfactant molecules as a function of time t for $(k_BT, \phi) = (0.9, 0.03)$ (gray line), (1,0.02) (black dashed line), (1,0.05) (blue line), and (1.2,0.08) (orange line).

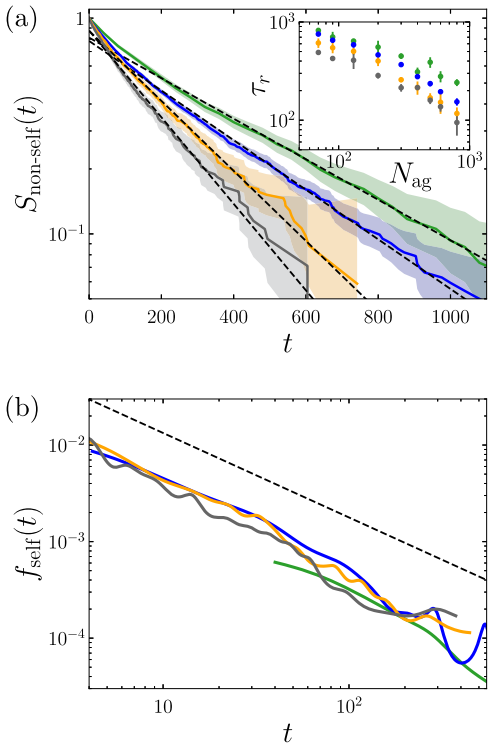

FIG. 5. (a) Survival function $S_{\text{non-self}}(t)$ for non-self-recombination with the 95% confidence interval and (b) the probability density function $f_{\text{self}}(t)$ of the recombination time for self-recombination with $N_{\text{ag}} = 300$ for $\delta t = \Delta t$ (gray), $10\Delta t$ (orange), $100\Delta t$ (blue), and $1000\Delta t$ (green). The inset in (a) shows the mean recombination time τ_r as a function of N_{ag}. The black dashed lines in (a) indicate an exponential fit to $S_{\text{non-self}}(t)$. The black dashed line in (b) indicates $f_{\text{self}}(t) \propto t^{-7/8}$.

shown in the inset of Fig. 5(a) is independent of δt. Furthermore, for self-recombination, the power law $f_{\text{self}}(t) \propto t^{-7/8}$ holds, irrespective of δt. Therefore, we conclude that the choice of δt does not change the qualitative characteristics of self-recombination or non-self-recombination. Thus, we use $\delta t = 100\Delta t$ to reduce the calculation cost.

B. Mean recombination time

In this subsection, we investigate the dependence of mean recombination time τ_r on the aggregation number, surfactant volume fraction, and temperature. We first examine the N_{ag} dependence of τ_r. Figure 6 shows τ_r as a function of N_{ag} for various ϕ and k_BT. Interestingly, as N_{ag} increases, the scaling law exhibits a transition from $\tau_r \propto N_{\text{ag}}^{-2/3}$ to $\tau_r \propto N_{\text{ag}}^{-1}$. We can qualitatively explain this crossover behavior by considering the micellar morphology. The gyration radius R_g of spherical micelles increases according to the power law $R_g \propto N_{\text{ag}}^{1/3}$ [see Fig. 13(a) from Ref. 29], indicating that their surface areas are proportional to $N_{\text{ag}}^{2/3}$. Therefore, τ_r of small micelles exhibits $\tau_r \propto N_{\text{ag}}^{-2/3}$ because of increase in the area where recombination can occur. In contrast, because wormlike micelles show one-dimensional growth, $\tau_r \propto N_{\text{ag}}^{-1}$ holds for large N_{ag}.

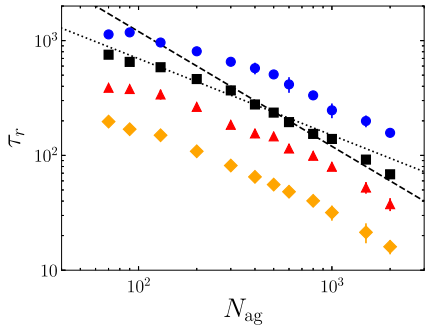

FIG. 6. Mean recombination time τ_r of micelles as a function of the aggregation number N_{ag} for $(k_BT, \phi) = (0.9, 0.05)$ (blue circle), (1,0.05) (black square), (1,0.08) (red triangle), and (1.1,0.1) (orange diamond). The black dotted line indicates $\tau_r \propto N_{\text{ag}}^{-2/3}$, and the black dashed line indicates $\tau_r \propto N_{\text{ag}}^{-1}$. The error bars denote the standard deviations for three independent simulations.

Next, we investigate the ϕ dependence of τ_r. Figure 7(a) shows τ_r as a function of ϕ for various N_{ag} values with fixed k_BT (=1). We find that τ_r is a decreasing function of ϕ. We have confirmed that ϕ has little effect on the diffusivity of the surfactants in dilute solutions (Fig. 4). Thus, it is reasonable to assume that an

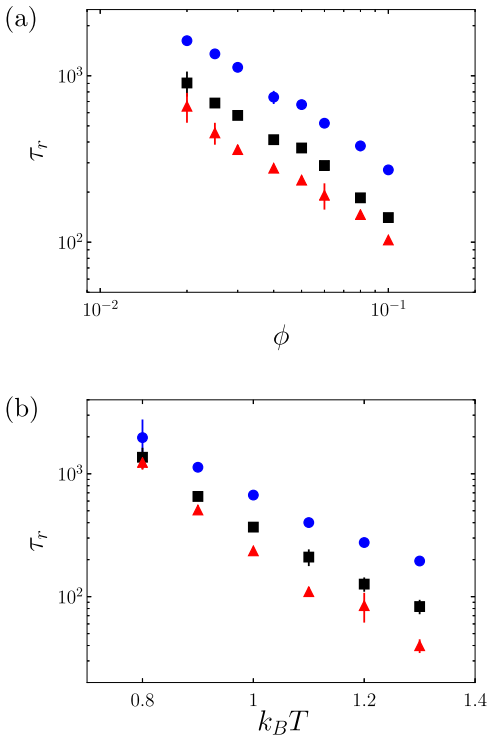

FIG. 7. Mean recombination time τ_r of micelles as a function of (a) the surfactant volume fraction ϕ with $k_BT = 1$ and (b) k_BT with $\phi = 0.05$ for $N_{\text{ag}} = 100$ (blue circle), 300 (black square), and 500 (red triangle). The error bars denote the standard deviations for three independent simulations.

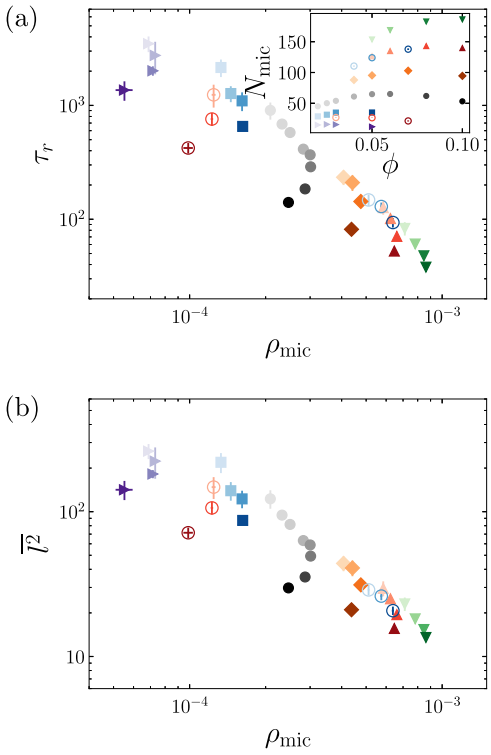

FIG. 8. (a) Mean recombination time τ_r and (b) mean squared diffusion distance $\overline{l^2}$ for recombination with $N_{ag} = 300$ as functions of the number density ρ_{mic} of micelles for $k_BT = 0.8$ (purple triangle), 0.9 (blue square), 1 (black circle), 1.1 (orange diamond), 1.2 (red triangle), and 1.3 (green triangle). Open symbols indicate the results of $a_{ht} = a_{tw} = 55$ (blue circle) and $a_{ht} = a_{tw} = 65$ (red circle) with $k_BT = 1$. Darker colors correspond to larger values of ϕ. The inset in (a) shows N_{mic} as a function of ϕ. The error bars in (a) and (b) denote the standard deviations for three independent simulations.

increase in the number of surfactants around the micelles results in a decrease in τ_r.

Finally, we investigate the k_BT dependence of τ_r. Figure 7(b) shows τ_r as a function of k_BT for several N_{ag} values with fixed ϕ (= 0.05). We find that τ_r is a decreasing function of k_BT, indicating that micellar recombination is promoted at high temperatures. An increase in k_BT leads to an increase in the diffusivity of surfactants (Fig. 4) and the number of micelles in the system [see the inset of Fig. 8(a)]. Thus, we infer that k_BT affects τ_r through the diffusivity and configuration of the micelles. These effects are discussed in detail in Sec. IV.

IV. DISCUSSION

In Sec. III B, we have evaluated τ_r for various N_{ag}, ϕ, and k_BT. Here, we explore a scaling law to explain the dependence of τ_r in an integrated manner. Because the N_{ag} dependence of τ_r and its physical interpretation have already been obtained in Fig. 6, we fix the value of N_{ag} at 300, for simplicity. We have confirmed that a common scaling law holds for at least $100 \lesssim N_{ag} \lesssim 600$.

We assume that τ_r is proportional to the average time required for surfactants in micelles to diffuse over the mean distance h between the nearest micelles. Under this assumption, the most important factors are the diffusivity of the surfactants and the configuration of the micelles. The activation energy may also play an essential role in recombination kinetics when considering different surfactants.[12] However, because we consider the same surfactant model in this study, we focus on the effects of diffusivity of surfactants and micellar configuration in the following discussion. A previous study[12] using a bead–spring model estimated h through the mean number density of chain ends. According to this concept, we obtain

$$h \propto \rho_{\mathrm{mic}}^{-1/3} \tag{3}$$

using the mean number density $\rho_{mic} = N_{mic}/V$ of micelles, where N_{mic} is the mean number of micelles in the system and V is the volume of the system. We observe that N_{mic} exhibits a complex dependence on ϕ and k_BT as shown in the inset of Fig. 8. To evaluate the effect of ρ_{mic} on τ_r, we show τ_r as a function of ρ_{mic} for various ϕ and k_BT values in Fig. 8(a). Although we can observe a slight correlation between τ_r and ρ_{mic}, ρ_{mic} cannot completely explain the behavior of τ_r. To consider the diffusivity of surfactants, we introduce the mean squared diffusion distance $\overline{l^2}$ for recombination, defined as $\overline{l^2} = \langle \Delta r^2(\tau_r) \rangle$. Here, $\sqrt{\overline{l^2}}$ indicates the characteristic length scale of surfactant diffusion until recombination. Figure 8(b) shows $\overline{l^2}$ as a function of ρ_{mic}. As indicated in Fig. 8(a), $\overline{l^2}$ also depends on parameters other than ρ_{mic}. The strong correlation between τ_r and ϕ for a fixed k_BT shown in Fig. 7(a) suggests that we must consider the explicit dependence on ϕ in addition to ρ_{mic}. In other words, ρ_{mic} alone cannot describe a micellar configuration.

We include the explicit dependence on ϕ to obtain a scaling law describing the characteristic time scale of micellar recombination. It is worth mentioning here that previous studies[12,14] assumed that recombination occurs only at chain ends. However, this assumption does not hold for considered micelles composed of surfactants because they can form branched structures (see Fig. 12 from Ref. 29). Therefore, the dependence of $\overline{l^2}$ cannot be explained by considering only ρ_{mic} [Fig. 8(b)]. Figure 9 shows τ_r and $\overline{l^2}$ as functions of $\rho_{mic}\phi$. Although we heuristically choose $\rho_{mic}\phi$ as a scaling variable, we find a power law describing the micellar recombination. As $\overline{l^2}$ includes the effect of diffusivity, Fig. 9(b) exhibits a clearer scaling than Fig. 9(a). Specifically, as shown in Fig. 9(b), $\overline{l^2} \propto (\rho_{mic}\phi)^{-2/3}$ is maintained, which is consistent with the scaling law obtained using Eq. (3) for fixed ϕ. In addition, $\tau_r \propto (\rho_{mic}\phi)^{-8/9}$ shown in Fig. 9(a) can be explained using $\overline{l^2} \propto (\rho_{mic}\phi)^{-2/3}$ and $\langle \Delta r^2(t) \rangle \propto t^{3/4}$ in the subdiffusion range, as shown in Fig. 4. Before closing this section, we have to mention the robustness of the scaling law. Figures 8 and 9 also show the results of $a_{ht} = a_{tw} = 55$ and $a_{ht} = a_{tw} = 65$ with the other conservative force coefficients unchanged. We find that the scaling law holds for different values of a_{ij}. However, we note that the scaling law does not include the effect of activation energy associated with recombination.[12] Therefore, it is an important area for future study to explore a more general scaling law of surfactants, including

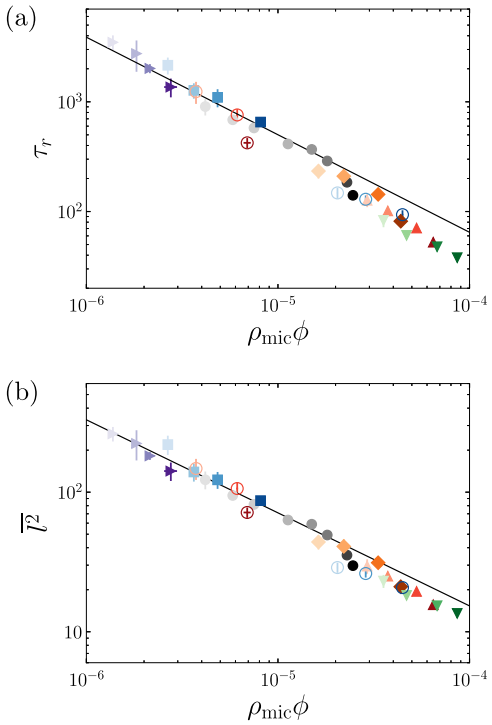

FIG. 9. (a) Mean recombination time τ_r and (b) mean squared diffusion distance $\overline{l^2}$ for recombination with $N_{\mathrm{ag}} = 300$ as functions of $\rho_{\mathrm{mic}}\phi$. The symbols are the same as in Fig. 8. The black line in (a) indicates $\tau_r \propto (\rho_{\mathrm{mic}}\phi)^{-8/9}$, and that in (b) indicates $\overline{l^2} \propto (\rho_{\mathrm{mic}}\phi)^{-2/3}$. The error bars in (a) and (b) denote the standard deviations for three independent simulations.

surfactants with different shapes and ionic surfactants. To summarize, we have obtained the scaling law for the mean recombination time of micelles in dilute surfactant solutions as a function of $\rho_{\mathrm{mic}}\phi$, although a theoretical derivation is left for a future study. Notably, the scaling law explains k_BT and ϕ dependence of τ_r (Fig. 7) using a single function (Fig. 9).

V. CONCLUSIONS

We conducted DPD simulations of nonionic surfactant solutions for various surfactant volume fractions ϕ and temperatures T to investigate the statistical properties of micellar recombination. We classified the recombination events into two categories: self-recombination, where two micelles produced through scission combine, and non-self-recombination. One of the most important conclusions is that the two recombination events have qualitatively different statistical properties. The survival function $S_{\text{non-self}}(t)$ for non-self-recombination obeys an exponential function [Fig. 3(a)], which indicates a mean-field picture. In contrast, the probability density function $f_{\mathrm{self}}(t)$ of the recombination time for self-recombination follows a power law [Fig. 3(b)], wherein the exponent is determined by the MSD of the surfactants (Fig. 4). These results are consistent with those of previous studies,[12,14] which used linear chains with a kinetic model for scission and recombination. It is worth noting that our DPD simulations do not impose any explicit assumption on the recombination kinetics. Therefore, we confirmed that these statistical laws also hold for micelles formed through the self-assembly of surfactants as well as for bead–spring models.

We also found a scaling law for the mean recombination time τ_r for non-self-recombination (Fig. 9). To obtain the scaling law, we evaluated τ_r for various N_{ag}, ϕ, and k_BT. For fixed ϕ and k_BT, τ_r shows $\tau_r \propto N_{\mathrm{ag}}^{-2/3}$ for small N_{ag} whereas $\tau_r \propto N_{\mathrm{ag}}^{-1}$ holds for large N_{ag} (Fig. 6), which corresponds to the structural transition from spherical to wormlike micelles. For a fixed N_{ag}, τ_r is a decreasing function of ϕ and k_BT (Fig. 7). To explain the dependence of τ_r on ϕ and k_BT in an integrated manner, we focused on the diffusivity of surfactants and the configuration of micelles. We showed that the mean number density ρ_{mic} of micelles is insufficient to describe the effect of micellar configurations on τ_r (Fig. 8). In addition, we must explicitly consider the effect of ϕ on τ_r. We then obtained the scaling law for τ_r as a function of $\rho_{\mathrm{mic}}\phi$ (Fig. 9). In previous studies,[12,14] it was assumed that recombination occurs only at chain ends and that the density of chain ends, which corresponds to ρ_{mic} in the present study, dominates the recombination rate. Thus, the necessity of ϕ in our scaling law in addition to ρ_{mic} comes from the complex recombination processes that were ruled out in previous studies.[12,14] In other words, we demonstrated more general recombination properties of surfactant micelles using DPD simulations.

In this study, we have paved the way for understanding the recombination phenomena of micelles by focusing on dilute nonionic surfactant solutions at equilibrium. There remain some issues to be addressed in future studies. First, our results are restricted to the case of a simple nonionic surfactant model. There are a lot of important micellar properties, including end-cap energy and stiffness.[3,25,38] In addition, counterions play an essential role in the properties of ionic surfactant micelles.[39,40] Thus, the framework presented here should be applied to other systems, which will lead to a more general understanding of the recombination process. Second, it is necessary to elucidate the recombination phenomena of micelles in flowing solutions, such as uniform shear and elongational flows. Microscopic knowledge of micellar recombination in nonequilibrium systems will help understand the rheological properties and develop constitutive models of micellar solutions.[41,42]

ACKNOWLEDGMENTS

The author is grateful to Professor S. Goto for valuable remarks on the first version of this manuscript. This study was supported in part by JSPS Grants-in-Aid for Scientific Research (Grant No. 21J21061). The DPD simulations were mainly conducted under the auspices of the NIFS Collaboration Research Programs (Grant No. NIFS20KNSS145). Some of the simulations were conducted using the JAXA Supercomputer System Generation 3 (JSS3).

AUTHOR DECLARATIONS

Conflict of Interest

The author has no conflicts to disclose.

Author Contributions

Yusuke Koide: Conceptualization (lead); Data curation (lead); Formal analysis (lead); Investigation (lead); Methodology (lead); Project administration (lead); Software (lead); Validation (lead); Visualization (lead); Writing – original draft (lead); Writing – review & editing (lead).

DATA AVAILABILITY

The data that support the findings of this study are available from the corresponding author upon reasonable request.

REFERENCES

[1] J. Yang, "Viscoelastic wormlike micelles and their applications," Curr. Opin. Colloid Interface Sci. **7**, 276–281 (2002).
[2] M. E. Cates and S. M. Fielding, "Rheology of giant micelles," Adv. Phys. **55**, 799–879 (2006).
[3] C. A. Dreiss, "Wormlike micelles: Where do we stand? Recent developments, linear rheology and scattering techniques," Soft Matter **3**, 956–970 (2007).
[4] M. E. Cates, "Reptation of living polymers: Dynamics of entangled polymers in the presence of reversible chain-scission reactions," Macromolecules **20**, 2289–2296 (1987).
[5] T. Shikata, H. Hirata, and T. Kotaka, "Micelle formation of detergent molecules in aqueous media: Viscoelastic properties of aqueous cetyltrimethylammonium bromide solutions," Langmuir **3**, 1081–1086 (1987).
[6] M. E. Cates and S. J. Candau, "Statics and dynamics of worm-like surfactant micelles," J. Phys.: Condens. Matter **2**, 6869–6892 (1990).
[7] T. Inoue, Y. Inoue, and H. Watanabe, "Nonlinear rheology of CTAB/NaSal aqueous solutions: Finite extensibility of a network of wormlike micelles," Langmuir **21**, 1201–1208 (2005).
[8] B. O'Shaughnessy and J. Yu, "Rheology of wormlike micelles: Two universality classes," Phys. Rev. Lett. **74**, 4329 (1995).
[9] I. A. Nyrkova and A. N. Semenov, "Correlation effects in dynamics of living polymers," Europhys. Lett. **79**, 66007 (2007).
[10] W. Zou, G. Tan, H. Jiang, K. Vogtt, M. Weaver, P. Koenig, G. Beaucage, and R. G. Larson, "From well-entangled to partially-entangled wormlike micelles," Soft Matter **15**, 642–655 (2019).
[11] S. Pahari, B. Bhadriraju, M. Akbulut, and J. S.-I. Kwon, "A slip-spring framework to study relaxation dynamics of entangled wormlike micelles with kinetic Monte Carlo algorithm," J. Colloid Interface Sci. **600**, 550–560 (2021).
[12] J. T. Padding and E. S. Boek, "Evidence for diffusion-controlled recombination kinetics in model wormlike micelles," Europhys. Lett. **66**, 756 (2004).
[13] M. Kröger and R. Makhloufi, "Wormlike micelles under shear flow: A microscopic model studied by nonequilibrium-molecular-dynamics computer simulations," Phys. Rev. E **53**, 2531 (1996).
[14] C.-C. Huang, H. Xu, and J.-P. Ryckaert, "Kinetics and dynamic properties of equilibrium polymers," J. Chem. Phys. **125**, 094901 (2006).
[15] S. Thakur, K. R. Prathyusha, A. P. Deshpande, M. Laradji, and P. B. S. Kumar, "Shear induced ordering in branched living polymer solutions," Soft Matter **6**, 489–492 (2010).
[16] N. Yoshii, K. Iwahashi, and S. Okazaki, "A molecular dynamics study of free energy of micelle formation for sodium dodecyl sulfate in water and its size distribution," J. Chem. Phys. **124**, 184901 (2006).
[17] R. Pool and P. G. Bolhuis, "Sampling the kinetic pathways of a micelle fusion and fission transition," J. Chem. Phys. **126**, 244703 (2007).
[18] N. Arai, K. Yasuoka, and Y. Masubuchi, "Spontaneous self-assembly process for threadlike micelles," J. Chem. Phys. **126**, 244905 (2007).
[19] S. Fujiwara, T. Itoh, M. Hashimoto, and R. Horiuchi, "Molecular dynamics simulation of amphiphilic molecules in solution: Micelle formation and dynamic coexistence," J. Chem. Phys. **130**, 144901 (2009).
[20] M. Velinova, D. Sengupta, A. V. Tadjer, and S.-J. Marrink, "Sphere-to-rod transitions of nonionic surfactant micelles in aqueous solution modeled by molecular dynamics simulations," Langmuir **27**, 14071–14077 (2011).
[21] A. V. Sangwai and R. Sureshkumar, "Binary interactions and salt-induced coalescence of spherical micelles of cationic surfactants from molecular dynamics simulations," Langmuir **28**, 1127–1135 (2012).
[22] R. Mao, M.-T. Lee, A. Vishnyakov, and A. V. Neimark, "Modeling aggregation of ionic surfactants using a smeared charge approximation in dissipative particle dynamics simulations," J. Phys. Chem. B **119**, 11673–11683 (2015).
[23] S. Dhakal and R. Sureshkumar, "Anomalous diffusion and stress relaxation in surfactant micelles," Phys. Rev. E **96**, 012605 (2017).
[24] F. Liu, D. Liu, W. Zhou, F. Chen, and J. Wei, "Coarse-grained molecular dynamics simulations of the breakage and recombination behaviors of surfactant micelles," Ind. Eng. Chem. Res. **57**, 9018–9027 (2018).
[25] S. Dhakal and R. Sureshkumar, "Topology, length scales, and energetics of surfactant micelles," J. Chem. Phys. **143**, 024905 (2015).
[26] P. J. Hoogerbrugge and J. M. V. A. Koelman, "Simulating microscopic hydrodynamic phenomena with dissipative particle dynamics," Europhys. Lett. **19**, 155 (1992).
[27] P. Español and P. Warren, "Statistical mechanics of dissipative particle dynamics," Europhys. Lett. **30**, 191 (1995).
[28] R. D. Groot and P. B. Warren, "Dissipative particle dynamics: Bridging the gap between atomistic and mesoscopic simulation," J. Chem. Phys. **107**, 4423–4435 (1997).
[29] Y. Koide and S. Goto, "Flow-induced scission of wormlike micelles in nonionic surfactant solutions under shear flow," J. Chem. Phys. **157**, 084903 (2022).
[30] Y. Koide and S. Goto, "Effect of scission on alignment of nonionic surfactant micelles under shear flow," Soft Matter **19**, 4323–4332 (2023).
[31] A. Vishnyakov, M.-T. Lee, and A. V. Neimark, "Prediction of the critical micelle concentration of nonionic surfactants by dissipative particle dynamics simulations," J. Phys. Chem. Lett. **4**, 797–802 (2013).
[32] M.-T. Lee, R. Mao, A. Vishnyakov, and A. V. Neimark, "Parametrization of chain molecules in dissipative particle dynamics," J. Phys. Chem. B **120**, 4980–4991 (2016).
[33] E. L. Kaplan and P. Meier, "Nonparametric estimation from incomplete observations," J. Am. Stat. Assoc. **53**, 457–481 (1958).
[34] J. D. Kalbfleisch and R. L. Prentice, *The Statistical Analysis of Failure Time Data* (John Wiley and Sons, 2011).
[35] C. Kim, B. U. Park, W. Kim, and C. Lim, "Bezier curve smoothing of the Kaplan-Meier estimator," Ann. Inst. Stat. Math. **55**, 359–367 (2003).
[36] B. H. Zimm, "Dynamics of polymer molecules in dilute solution: Viscoelasticity, flow birefringence and dielectric loss," J. Chem. Phys. **24**, 269–278 (1956).
[37] M. Rubinstein and R. H. Colby, *Polymer Physics* (Oxford University Press, 2003).
[38] C. Oelschlaeger, P. Suwita, and N. Willenbacher, "Effect of counterion binding efficiency on structure and dynamics of wormlike micelles," Langmuir **26**, 7045–7053 (2010).
[39] P. Mukerjee, K. Mysels, and P. Kapauan, "Counterion specificity in the formation of ionic micelles - size, hydration, and hydrophobic bonding effects," J. Phys. Chem. **71**, 4166–4175 (1967).
[40] R. Abdel-Rahem, "The influence of hydrophobic counterions on micellar growth of ionic surfactants," Adv. Colloid Interface Sci. **141**, 24–36 (2008).
[41] S. Tamano, S. Hamanaka, Y. Nakano, Y. Morinishi, and T. Yamada, "Rheological modeling of both shear-thickening and thinning behaviors through constitutive equations," J. Non-Newtonian Fluid Mech. **283**, 104339 (2020).
[42] R. J. Hommel and M. D. Graham, "Constitutive modeling of dilute wormlike micelle solutions: Shear-induced structure and transient dynamics," J. Non-Newtonian Fluid Mech. **295**, 104606 (2021).